DE GRUYTER OPEN

Synthesis and electrical characterization of $Ca_2Nd_4Ti_6O_{20}$ ceramics

RAZ MUHAMMAD[1,3]*, MUHAMMAD UZAIR[2], M. JAVID IQBAL[2], M. JAWAD KHAN[2], YASEEN IQBAL[2], CARLOS R. RAMBO[3]

[1]Department of Physics, Islamia College Peshawar, 25120, Khyber Pakhtunkhwa, Pakistan

[2]Department of Physics, University of Peshawar, 25120, Khyber Pakhtunkhwa, Pakistan

[3]Laboratory of Electrical Materials, Federal University of Santa Catarina, Florianopolis, Brazil

$Ca_2Nd_4Ti_6O_{20}$, a layered perovskite structured material was synthesized via a chemical (citrate sol-gel) route for the first time using nitrates and alkoxide precursors. Phase analysis of a sample sintered at 1625 °C revealed the formation of an orthorhombic (Pbn21) symmetry. The microstructure of the sample after sintering comprised rod-shaped grains of a size of 1.5 to 6.5 µm. The room temperature dielectric constant of the sintered sample was 38 at 100 kHz. The remnant polarization (P_r) and the coercive field (E_c) were about 400 µC/cm^2 and 8.4 kV/cm, respectively. Impedance spectroscopy revealed that the capacitance (13.7 pF) and activation energy (1.39 eV) of the grain boundary was greater than the capacitance (5.7 pF) and activation energy (1.13 eV) of the grain.

Keywords: *sol-gel; $Ca_2Nd_4Ti_6O_{20}$; electrical properties*

1. Introduction

Perovskite-type structure materials exhibit interesting physical, chemical and electrical properties [1]. Among these, $A_nB_nO_{3n+2}$-type perovskites were investigated in 1972 by Galy et al. [2] followed by comprehensive crystallographic studies by various researchers [3–6]. Layered $A_nB_nO_{3n+2}$-type perovskites are derived from ABO_3, where n denotes the number of octahedral slabs comprising $n[BO_6]$ octahedra within the unit cell. Ferroelectricity was discovered in the layered perovskite-like structures and $Sr_2Ta_2O_7$ ($A_nB_nO_{3n+2}$, n = 4) was claimed to be the first ferroelectric [7]. Similarly, other oxides of $A_nB_nO_{3n+2}$ (n = 4) which are non-centrosymmetric, such as $A_2Nb_2O_7$ (A = Ca, Sr) and $Ln_2Ti_2O_7$ (Ln = La, Nd), comprise the ferroelectrics with the highest Curie temperature (T_c) [8]. In general, the oxides with n = 2, 3 (II), 4 and 6 are non-centrosymmetric and exhibit

ferroelectricity while the uneven types, n = 3 (I), n = 5 or n = 7 are centrosymmetric [8, 9]. $Ca_2Nd_4Ti_6O_{20}$ (CNT) is a non-centrosymmetric compound which belongs to $A_nB_nO_{3n+2}$ family (with A = Nd, Ca, B = Ti and n = 6). In this compound calcium and neodymium occupy the same crystallographic sites. Among the methods to produce non-centrosymmetric CNT, the sol-gel route is a versatile and advantageous method to produce very fine and more homogenous powders than those produced by the mixed-oxide route [10, 11]. In this study, the sol-gel method was employed for the first time to synthesize CNT powder sample and the final ceramics were characterized in terms of phase, microstructure and electrical properties.

2. Experimental

The CNT compound was prepared using $Ca(NO_3)_2 \cdot 4H_2O$, $Nd(NO_3) \cdot 6H_2O$ and Ti-butoxide ($C_{16}H_{36}O_4Ti$) as sol-gel precursors. Appropriate amounts of $Ca(NO_3)_2 \cdot 4H_2O$ and $Nd(NO_3)_2 \cdot 6H_2O$ were dissolved in ethanol (C_2H_5OH) and stirred

*E-mail: razmohammad_phy@yahoo.com

vigorously to form a solution "A". Ti-butoxide, ethanol, water (H$_2$O), nitric acid (HNO$_3$) and acetic acid (CH$_3$COOH) were mixed according to the volumetric ratios [12] given in Table 1, to form solution "B". Solutions A and B were mixed and stirred for 8 h. The viscous liquid was dried at 80 °C to form brown ash powders. The obtained powders were calcined in an alumina boat at 1150 °C for 6 h with a heating/cooling rate of 10 °C/min. The calcined powders were re-milled using a mortar and a pestle to reduce the particle size in order to enhance sinterability. The powders were pressed into cylindrical-shaped pellets, using a 10 mm diameter steel die at 50 MPa and sintered at temperatures ranging from 1450 to 1650 °C for 4 h at a heating/cooling rate of 5 °C/min. The density of sintered pellets was measured using a MD-300s densitometer, based on Archimedes principle.

Table 1. The volumetric ratios of chemical compositions.

Ti	Ethanol	Acetic acid	HNO$_3$	H$_2$O
20 %	80 %	6 %	3 %	3 %

A Siemens D5000 X-ray diffractometer (CuKα radiation) was used for phase analysis of the calcined and sintered powders. The microstructure of a finely polished, thermally etched and gold coated sample was examined using an FEI Inspect-F scanning electron microscope. For electrical properties measurements, the opposite surfaces of sintered pellets were coated with gold paste and fired at 800 °C for 2 h. Permittivity and dielectric losses from 100 kHz to 1 MHz were measured using a precision LCR meter (4284 A) with an applied AC voltage of 100 mV from room temperature up to 700 °C in air. Polarization-electric field (P-E) hysteresis loop measurements were made at room temperature in silicone oil using a Radiant Technology RT-66A standardized ferroelectric test system and Trek 609E-6 high voltage amplifier. These measurements were performed at a maximum applied voltage of 20 kV/cm. Impedance spectroscopy of the sample was carried out using an HP-4192A impedance analyzer

(Agilent Technologies) from room temperature to 800 °C.

3. Results and discussion

X-ray diffraction pattern of a CNT sample sintered at 1625 °C is shown in Fig. 1. The Bragg's reflections of the XRD peaks were matched PDF# 070-0200 for orthorhombic CNT. No evidence of secondary phase formation was observed within the detection limit of the in-house XRD facility. The refined lattice parameters, using X'Pert High Score Plus software were measured to be a = 7.664 Å, b = 36.967 Å, c = 5.432 Å and V = 1538.9 Å^3.
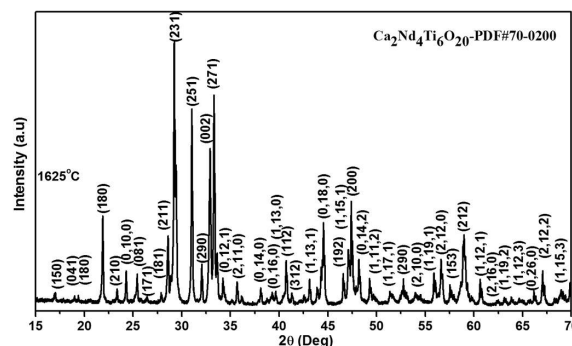

Fig. 1. X-ray diffraction pattern of CNT sintered at 1625 °C.

The relative density of the sample increased with increasing temperature from 1450 to 1625 °C and then decreased upon a further increase in temperature to 1650 °C. The relative density of the sample sintered at the optimum sintering temperature (1625 °C) was measured to be 92 %. A typical secondary electron SEM micrograph of the CNT sample sintered at 1625 °C for 4 h is shown in Fig. 2. The microstructure comprised elongated rod-shaped grains of the size ranging from 1.5 μm to 6.5 μm. The energy X-ray spectroscopy (EDS) analyses of some of the grains (labeled as a, b and c) are given in Table 2. The analysis revealed that the composition of all the grains was similar, which indicates chemical homogeneity of the sample.

The temperature dependent dielectric constant and dielectric loss for CNT sample sintered at
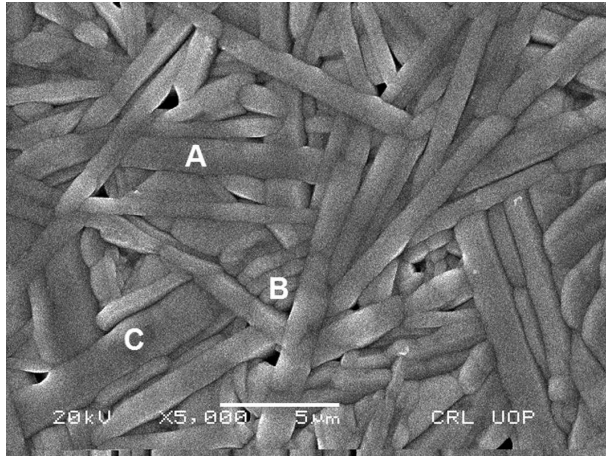
Fig. 2. Secondary electron SEM micrograph of CNT sintered at 1625 °C.

Table 2. EDX data of CNT sample sintered at 1625 °C.

Elements	Ca [wt.%]	Ti [wt.%]	Nd [wt.%]
Grain (A)	7.2	29.1	63.7
Grain (B)	7.9	30.3	61.7
Grain (C)	7.4	29.8	62.8

Fig. 3. Temperature dependence of ε_r and tanδ of CNT sample measured at different frequencies.

Fig. 4. P-E hysteresis loop of CNT sample.

1625 °C is shown in Fig. 3. The dielectric constant increased from 38 to 96 at 100 KHz with an increase in temperature from room temperature to 700 °C. The increase in dielectric constant at high temperatures might have originated from the high temperature charge conductivity [13]. Similarly, the dielectric loss also increased from 0.006 to 0.95 (100 kHz) with increasing temperature from 30 to 700 °C. No phase transition was observed because these materials have a very high T_c [8, 9]. Fig. 4 shows the ferroelectric hysteresis loop of a CNT sample at room temperature at an external field of 10 kV/cm. The remnant polarization (P_r) and the coercive field (E_c) are ∼400 μC/cm^2 and 8.4 kV/cm, respectively. Such high P_r value may be attributed to the presence of abundant space charge which does not reflect the intrinsic ferroelectricity of this material.

The Nyquist plots (real part Z' of complex impedance versus imaginary part $-Z''$ of complex impedance) measured for the CNT sample is shown in Fig. 5a, where the arrow (ω) re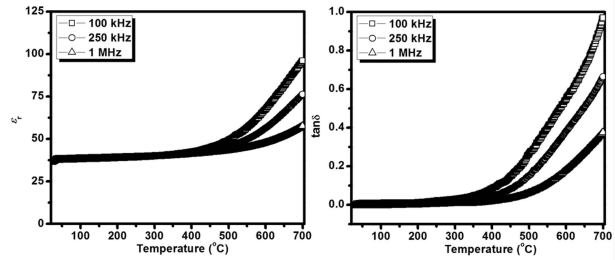presents the increase in frequency. The arcs formed at each temperature showed distorted semicircles which can be attributed to the overlapping of the two electroactive regions. The resistivity of the sample decreased with an increase in temperature as indicated by the decreasing trend in the radius of the semicircular arc. The spectroscopic plots ($-Z''$ versus log f) in Fig. 5b, exhibited shifting of the peaks towards relatively higher frequency with increasing temperature, which indicates an increase in the mobility of charge carriers in the CNT ceramics [14]. The asymmetrical nature of the peaks suggested the non-Debye type behavior of the sample. The broadening of the peaks also confirmed that the two electro-active regions overlapped due to the relaxation time shorter than 10^{-2} s. To probe the electrically inhomogeneous nature of CNT ceramics, which has different electroactive regions, the combined spectroscopic plots of the imaginary components of impedance Z'' and electric modulus M'' were used (Fig. 6).
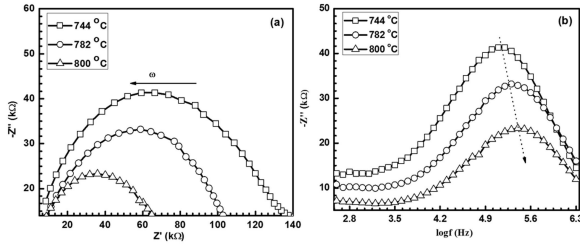
Fig. 5. (a) Plot of real part Z' vs. imaginary part $-Z''$ of the complex impedance $Z*$ (b) spectroscopic plot of Z'' and log f at different temperatures.

A single relaxation occurs at 125.89 kHz, 199.53 kHz and 251.19 kHz for 744, 782 and 800 °C, respectively. Similarly, in the modulus formalism one relaxation was observed for each temperature, i.e. at 794.33 kHz, 1000 kHz and 1258.9 kHz for 744, 782 and 800 °C, respectively. This is in accordance with the general principle that the capacitance decreases with increasing frequency [15, 16]. R and C values were calculated from the peaks in the Z'' spectroscopic plots using f_{max} value of the peak, i.e. $R_{gb} = 2 Z''$ and the relationship $2\pi f_{max}RC = 1$ at the peak maximum, respectively [17]. In Fig. 6, the peaks in the Z'' spectra have an associated resistance and capacitance values as given in Table 3. It is evident from Table 3 that by increasing the temperature, the value of resistance of both the grain and grain boundary decreases.

Fig. 6. Spectroscopic plots of impedance Z'' and modulus M'' at temperatures (a) 744 °C (b) 782 °C and (c) 800 °C.

Fig. 7. Plots of frequency dependence of capacitance of grain and grain boundary regions at different temperatures.

Table 3. Values of R and C extracted from Z''_{max} and from M''_{max}.

Temp. [°C]	R_{gb} [kΩ] Extracted	C_{gb} [pF] from Z''_{max}	R_g [kΩ] Extracted	C_g [pF] from M''_{max}
744	92.13	13.72	35.080	5.71
782	73.82	13.57	28.133	5.70
800	51.03	12.41	22.190	5.66

Fig. 7 shows the capacitance versus frequency response, which confirms the presence of two electroactive regions (i.e. grain and grain boundary). At low frequencies, the grain boundary response is dominant whereas the emergence of bulk is 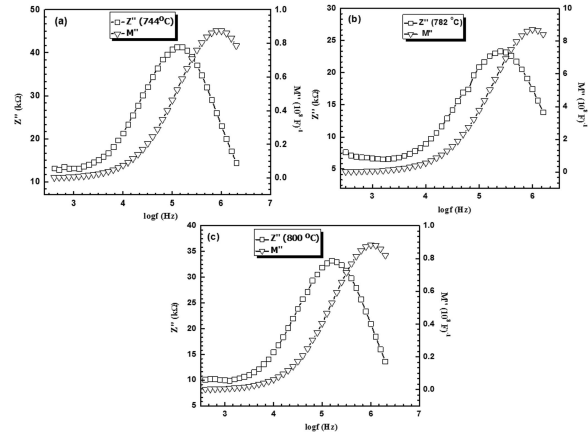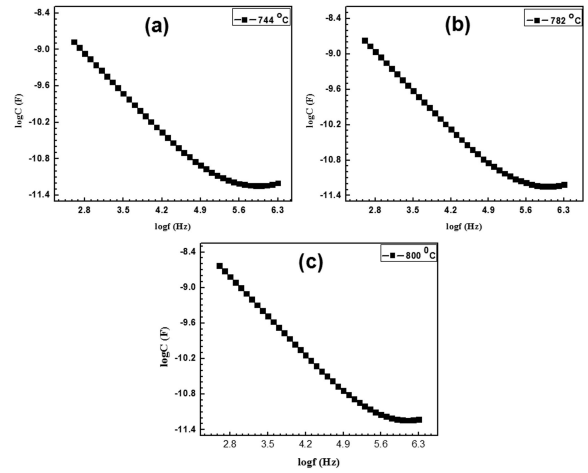observed at higher frequencies. As the temperature was lowered to 744 °C the grain boundary region shifted to low frequency values and the grain effect was more pronounced. The conductivity of CNT linearly increased with an increase in temperature and the activation energies of the grain and grain boundary were found to be 1.13 eV and 1.39 eV, respectively. By comparing their activation energies, it can be suggested that in the given temperature range, the bulk (or grain) is less resistive than the grain boundary in the CNT sample. The grain and grain boundary regions having different thermal activation energies suggest

two different transport mechanisms in the investigated CNT sample.

4. Conclusion

Single phase CNT ceramics with an orthorhombic (Pbn21) structure were synthesized via sol-gel route. The microstructure of the sintered ceramics comprised elongated rod-shaped grains of the length ranging from 1.5 to 6.5 µm. Dielectric constant versus temperature plots did not show phase transition in the temperature range between 30 °C and 700 °C. Impedance spectroscopy analysis indicated two overlapped electroactive regions (i.e. grain and grain boundary). The resistance of both the grain and grain boundary was observed to increase with temperature. Furthermore, the activation energy of the grain was less than the activation energy of grain boundaries.

References

[1] BHALLA A., GUO R., ROY R., *Mater. Res. Inno.*, 4 (2000), 3.

[2] GALY J., CARPY A., *Phil. Mag.*, 29 (1974), 1207.

[3] PORTIER R., FAYARD M., CARPY A., GALY J., *Mater. Res. Bull.*, 9 (1974), 371.

[4] NANOT M., QUEYROUX F., GILLES J.-C., PORTIER R., *J. Sol. Sci. Tech.*, 38 (1981), 74.

[5] NANOT M., QUEYROUX F., GILLES J., CAPPONI J., *J. Sol. Sci. Tech.*, 61 (1986), 315.

[6] LEVIN I., BENDERSKY L.A., VANDERAH T.A., ROTH R.S., STAFSUDD O.M., *Mater. Res. Bull.*, 33 (1998), 501.

[7] ISUPOV V., *Ferroelectrics*, 220 (1999), 79.

[8] LICHTENBERG F., HERRNBERGER A., WIEDENMANN K., *Prog. Sol. St. Chem.*, 36 (2008), 253.

[9] LICHTENBERG F., HERRNBERGER A., WIEDENMANN K., MANNHART J., *Prog. Sol. St. Chem.*, 29 (2001), 1.

[10] HSIAO Y.J., CHANG Y.H., CHANG Y.S., FANG T.H., *J. Am. Ceram. Soc.*, 90 (2007), 2287.

[11] LI J., QIU T., FAN C., XU P., *J. Sol. Sci. Tech.*, 59 (2011), 525.

[12] JIN S., XIA H., ZHANG Y., GUO J., XU J., *Mater. Lett.*, 61 (2007), 1404.

[13] CHEN X., LU Y., JIN D., LIU X., *J. Electroceram.*, 15 (2005), 21.

[14] IDREES M., NADEEM M., HASSAN M.M., *J. Phys. D*, 43 (2010), 155401.

[15] APARNA M., BHIMASANKARAM T., SURYANARAYANA S., PRASAD G., KUMAR G., *Bull. Mater. Sci.*, 24 (2001), 497.

[16] UZAIR M., IQBAL Y., MUHAMMAD R., HAYAT K., REANEY I.M., *J. Mater. Sci.*, 50 (2015), 1752.

[17] IRVINE J.T., SINCLAIR D.C., WEST A.R., *Adv. Mater.*, 2 (1990), 132.